PCP
PLANT & CELL PHYSIOLOGY

Special Issue – Regular Paper

Control of Plant Cell Growth and Proliferation by MO25A, a Conserved Major Component of the Mammalian Sterile 20–Like Kinase Pathway

Kim Nhung Ta[1,6,†], Mari W. Yoshida[2,†], Takumi Tezuka[3], Sae Shimizu-Sato[1], Misuzu Nosaka-Takahashi[1,3], Atsushi Toyoda[1], Takamasa Suzuki[4], Gohta Goshima[2,5,*] and Yutaka Sato[1,3,*]

[1]Department of Genome and Evolutionary Biology, National Institute of Genetics, 1111 Yata, Mishima, Shizuoka, 411-8540 Japan
[2]Department of Biological Science, Graduate School of Science, Nagoya University, Furo-cho, Chikusa-ku, Nagoya, 464-8602 Japan
[3]Department of Genetics, School of Life Science, SOKENDAI (Graduate University for Advanced Studies), 1111 Yata, Mishima, Shizuoka, 411-8540 Japan
[4]College of Bioscience and Biotechnology, Chubu University, 1200 Matsumoto-cho, Kasugai, Aichi, 487-8501 Japan
[5]Sugashima Marine Biological Laboratory, Graduate School of Science, Nagoya University, 429-63 Sugashima, Toba, 517-0004 Japan
[6]Present address: Vietnam Japan University, Vietnam National University, Hanoi, Vietnam.
[†]These authors contributed equally to this work.

*Corresponding authors: Gohta Goshima, E-mail, goshima@bio.nagoya-u.ac.jp; Yutaka Sato, E-mail, yusato@nig.ac.jp

(Received 21 August 2022; Accepted 12 January 2023)

The precise control of cell growth and proliferation underpins the development of plants and animals. These factors affect the development and size of organs and the body. In plants, the growth and proliferation of cells are regulated by environmental stimuli and intrinsic signaling, allowing different cell types to have specific growth and proliferation characteristics. An increasing number of factors that control cell division and growth have been identified. However, the mechanisms underlying cell type–specific cell growth and proliferation characteristics in the normal developmental context are poorly understood. Here, we analyzed the rice mutant *osmo25a1*, which is defective in the progression of embryogenesis. The *osmo25a1* mutant embryo developed incomplete embryonic organs, such as the shoot and root apical meristems. It showed a delayed progression of embryogenesis, associated with the reduced mitotic activity. The causal gene of this mutation encodes a member of the Mouse protein-25A (MO25A) family of proteins that have pivotal functions in a signaling pathway that governs cell proliferation and polarity in animals, yeasts and filamentous fungi. To elucidate the function of plant MO25A at the cellular level, we performed a functional analysis of MO25A in the moss *Physcomitrium patens*. *Physcomitrium patens* MO25A was uniformly distributed in the cytoplasm and functioned in cell tip growth and the initiation of cell division in stem cells. Overall, we demonstrated that MO25A proteins are conserved factors that control cell proliferation and growth.

Keywords: MO25 • Morphogenesis-related NDR kinase pathway • *Physcomitrium* (*Physcomitrella*) *patens* • Rice • Stem cells

Introduction

Plant development relies on a highly coordinated process of cell proliferation and enlargement. The rate of cell proliferation and the degree of cell enlargement depend on the cell type. The direction of division and elongation and their regulation by internal and external cues affect the development and size of individuals and organs. Cells that make up the plant body belong to the basic tissue system which is formed during embryogenesis. They are continuously produced after embryogenesis by stem cells or populations of stem cells, which are produced during embryogenesis. In seed plants, stem cell populations are located at the tips of the above- and below-ground parts of the plant body, and these are called shoot apical meristems (SAMs) and root apical meristems (RAMs), respectively. Various specialized cells are produced in SAMs and RAMs, which have their specific cell proliferation and enlargement characteristics that are essential for the normal developmental progression of plant organs. Indeed, in angiosperms, the central and peripheral zones of SAMs have different mitotic activities, and abnormalities in mitotic activity in this region have a major impact on plant development (Davis et al. 1979, Itoh et al. 2000, Reddy et al. 2004, Nosaka-Takahashi et al. 2022).

Plant Cell Physiol. 64(3): 336–351 (2023) doi:https://doi.org/10.1093/pcp/pcad005, Advance Access publication on 13 January 2023, available online at https://academic.oup.com/pcp

The effects of changes in cell proliferation frequency due to mutation or genetic manipulation on plant development have been well studied (reviewed in Jakoby and Schnittger 2004, Inzé and De Veylder 2006). For example, the expression of the dominant-negative form of *Arabidopsis cdc2a* in embryos affects embryo patterning and organogenesis (Hemerly et al. 2000). *Arabidopsis tilted1* (*til1*) has a mutation in a gene encoding a DNA polymerase holoenzyme, which is involved in DNA replication. Strong alleles of *til1* are embryo-lethal (Ronceret et al. 2005), whereas weak alleles cause a prolonged cell cycle and affect embryonic patterning (Jenik et al. 2005). However, cell enlargement may have a compensatory effect on the growth of organs such as leaves when the frequency of cell division is reduced due to mutations (Horiguchi and Tsukaya 2011).

In metazoans, the Hippo/Mammalian Sterile 20-like (MST) kinase pathway, also known as the morphogenesis-related nuclear dbf2-related (NDR) kinase (MOR) pathway (Maerz and Seiler 2010, Zhao et al. 2011, Thompson and Sahai 2015), operates as a major signaling pathway that regulates cell proliferation, polarity and cell-type specification in concert and determines the size of the body and organs. The pathway components are conserved widely among eukaryotes, including unicellular yeasts. In budding yeast, the germinal center kinase Kic1 (equivalent to MST kinases in mammals), NDR kinase Cbk1 (NDR1 and NDR2 in mammals) and their associated regulatory proteins Mob (MOB1 and MOB2 in mammals), kinase scaffolding proteins Hym1/Mo25 and Tao3 (FRYa in mammals) and Sog2, which regulate Kic1 activity, are major components of this pathway (Maerz and Seiler 2010, Bizotto et al. 2018). In the MST pathway, Kic1, activated by the kinase scaffold proteins Hym1/Mo25 and Sog2, phosphorylates Cbk1, which forms a complex with Mob via Tao3. Thus, activated Cbk1 phosphorylates downstream targets, such as Ace2, a transcription factor that functions in cell separation in budding yeast (Oud et al. 2013). In metazoans, malfunctions of this pathway are known to cause a wide range of abnormalities related to cell proliferation and polarity, stem cell activity, organ size and tissue regeneration (Bidlingmaier et al. 2001, Nelson et al. 2003, Kanai et al. 2005, Mendoza et al. 2005, ten Klooster et al. 2009, Dettmann et al. 2012, Chien et al. 2013). Components of this pathway are also well conserved in plants, and co-expression data suggest that these factors are involved in cell polarity, including tip growth (Zermiani et al. 2015).

In plants, signaling that governs cell proliferation and expansion intrinsic to embryo development and cellular specification at the SAM and RAM are not understood. Mutations that affect cell proliferation and elongation are likely to affect embryogenesis, causing embryonic lethality, as in *til1*. Systematic collections and analyses of embryogenesis-defective mutant lines have been reported for *Arabidopsis* and rice (Hong et al. 1995, Meinke 2020). In this study, we focused on a mutant obtained from a series of rice embryogenesis-defective mutant lines in which the differentiation of SAMs and RAMs becomes obscured during embryogenesis. We showed that embryogenesis in the mutant is delayed due to reduced mitotic activity, resulting in incomplete organ differentiation at the time of seed maturation. The mutation was identified in the gene encoding the plant MO25A protein. To elucidate the function of plant MO25A at the cellular level, we performed a functional analysis of MO25A in the basal land plant *Physcomitrium patens* and observed that it functions in the proliferation and branch formation of stem cells.

Results

Mutations in the *OsMO25A* gene cause defective development of rice embryos

Screening of mutant rice embryos with defective organogenesis resulted in identifying a mutant line, *08T6S44*, that segregated mutant embryos with incomplete organ differentiation (**Fig. 1A, B**). Seeds with mutant embryos did not germinate, suggesting embryo lethality owing to this mutation. The mutant embryos were segregated in a single recessive inheritance manner after self-pollinations of heterozygous parents, and the heterozygotes were morphologically indistinguishable from wild-type (WT) plants. We identified a candidate causal gene for this mutation by combining map-based cloning and next-generation sequencing (Suzuki et al. 2018). In brief, we conducted rough mapping using the F2 population and found that the mutation resides around the 24-Mb position of chromosome 7. Next, we extracted genomic DNA from bulked seedlings using seed sets from heterozygous parents and conducted next-generation sequencing. As parents were maintained for years by multiple self-pollinations, it is expected that most genomic regions, other than the region covering the mutant locus, were fixed in the homozygote. Thus, we searched for heterozygous blocks in the mutant genome and observed a 12-Mb heterozygous region on chromosome 7, where rough mapping suggested the position of the mutation (**Supplementary Fig. S1**). Within this region, the only nonsense mutation was found in the gene encoding a protein named OsMO25A (locus IDs: Os07g0585100, The Rice Annotation Project Database (RAP-DB); LOC_Os07g39630, Michigan State University Rice Genome Annotation Project (MSU)).

MO25 is a protein conserved among eukaryotes and is known to act as a kinase scaffold for the MOR pathway (Weiss et al. 2002, Maerz and Seiler 2010, Saputo et al. 2012, Weiss 2012). In plants, MO25 family genes are classified into two groups (MO25A and MO25B) (**Supplementary Fig. S2**) (Zermiani et al. 2015, Bizotto et al. 2018). OsMO25A1 and OsMO25A2 belong to the MO25A group, whereas rice contains two other genes that are more similar to MO25B (**Supplementary Fig. S2**). The critical residues for the activation of MST3 kinase, one of the major kinases in the MOR pathway (Tyr223, Arg227 and Met260 in human MO25α), are conserved in AtMO25s and OsMO25s, suggesting that plant MO25 may also act as a scaffold for kinase signaling (Filippi et al. 2011, Mehellou et al. 2013, Bizotto et al. 2018). However, genetic perturbations have not been reported in plant *MO25* genes.

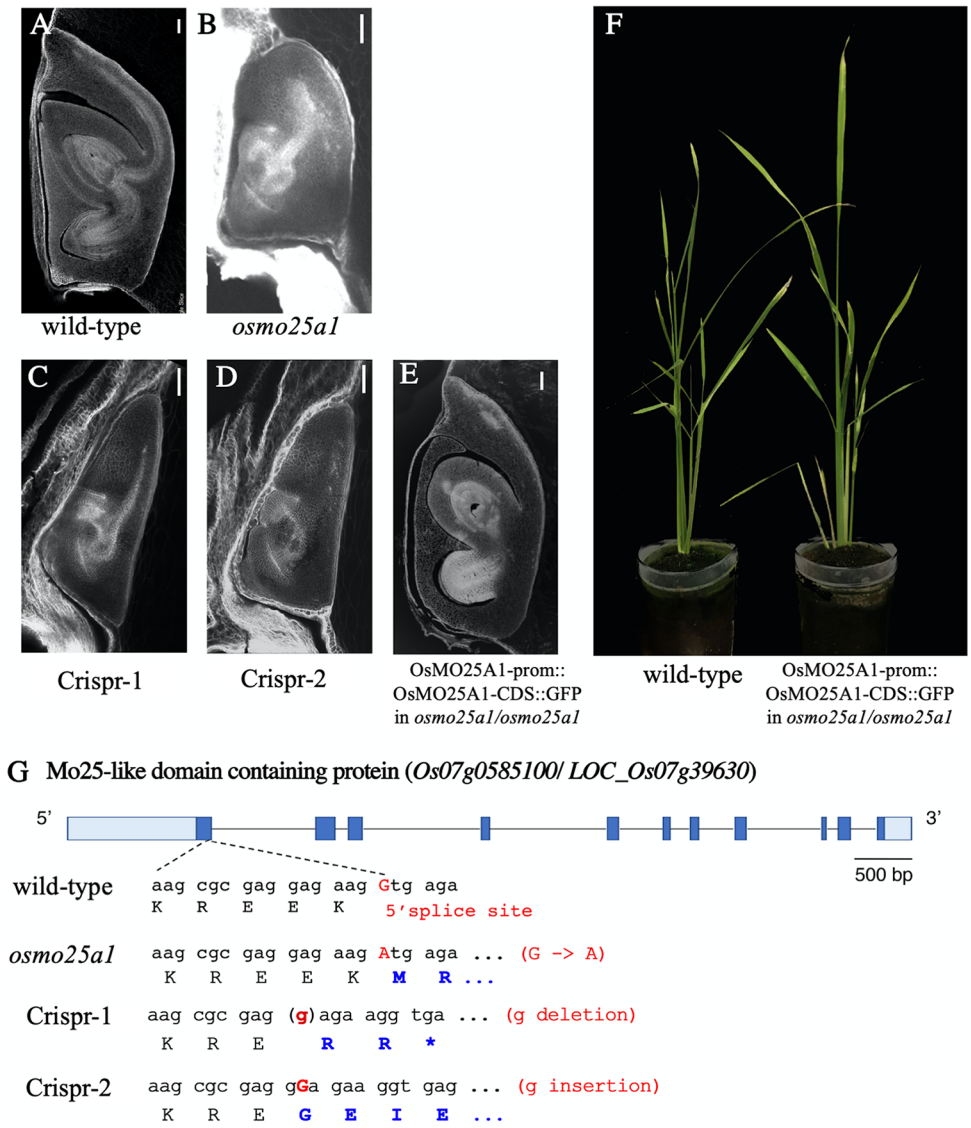

Fig. 1 Mutations in the *OsMO25A1* gene cause defective embryo development. (A–D) Morphology of embryos from WT, 08T6S44, Crispr-1 and Crispr-2 (A–D). (E, F) Morphology of an embryo (E) and a plant (F) expressing OsMO25A1::GFP fusion protein under the OsMO25A1 promoter in the background of homozygous *osmo25a1* mutation. (G) *OsMO25A1* gene structure and mutations in *osmo25a1* and Crispr-1 and Crispr-2 lines.

To confirm that *OsMO25A1* is the causal gene of this mutation, we created two new allelic mutations using CRISPR/Cas9, which carried a single nucleotide insertion and deletion, respectively, in the candidate gene. Among the regenerated plants, we obtained only monoallelic mutations, possibly due to the lethality or slow growth of calli caused by biallelic mutations, as is often the case for genes responsible for embryo development. Thus, the regenerated plants were heterozygous for the mutant alleles. After self-pollination, both lines carrying new alleles segregated mutant embryos, indistinguishable from mutant embryos segregating in *08T6S44* (**Fig. 1B–D, G**). Furthermore, a molecular complementation experiment using *OsMO25A1* cDNA fused with GFP and the *OsMO25A1* promoter recovered homozygous mutant seeds with normal embryo morphology; they germinated and grew normally until maturity (**Fig. 1E, F**). Based on these results, we concluded that *OsMO25A1* is the causal gene for this mutation. Hereafter, the allele-segregating mutant embryos from the *08T6S44* line are named *osmo25a1* (**Fig. 1G**).

Delayed embryo development and low mitotic activity in the *osmo25a1* mutant embryo

To gain insights into the incomplete organ formation of *osmo25a1* mutation, we observed the developmental course of mutant and WT embryos at six major stages of WT embryo development, including Em4 at 3 d after pollination (DAP) (late globular), Em5 at 4 DAP (onset of coleoptile, SAM and radicle differentiation), Em6 at 5 DAP (formation of the first leaf primordium), Em7 at 7 and 8 DAP (formation of the second

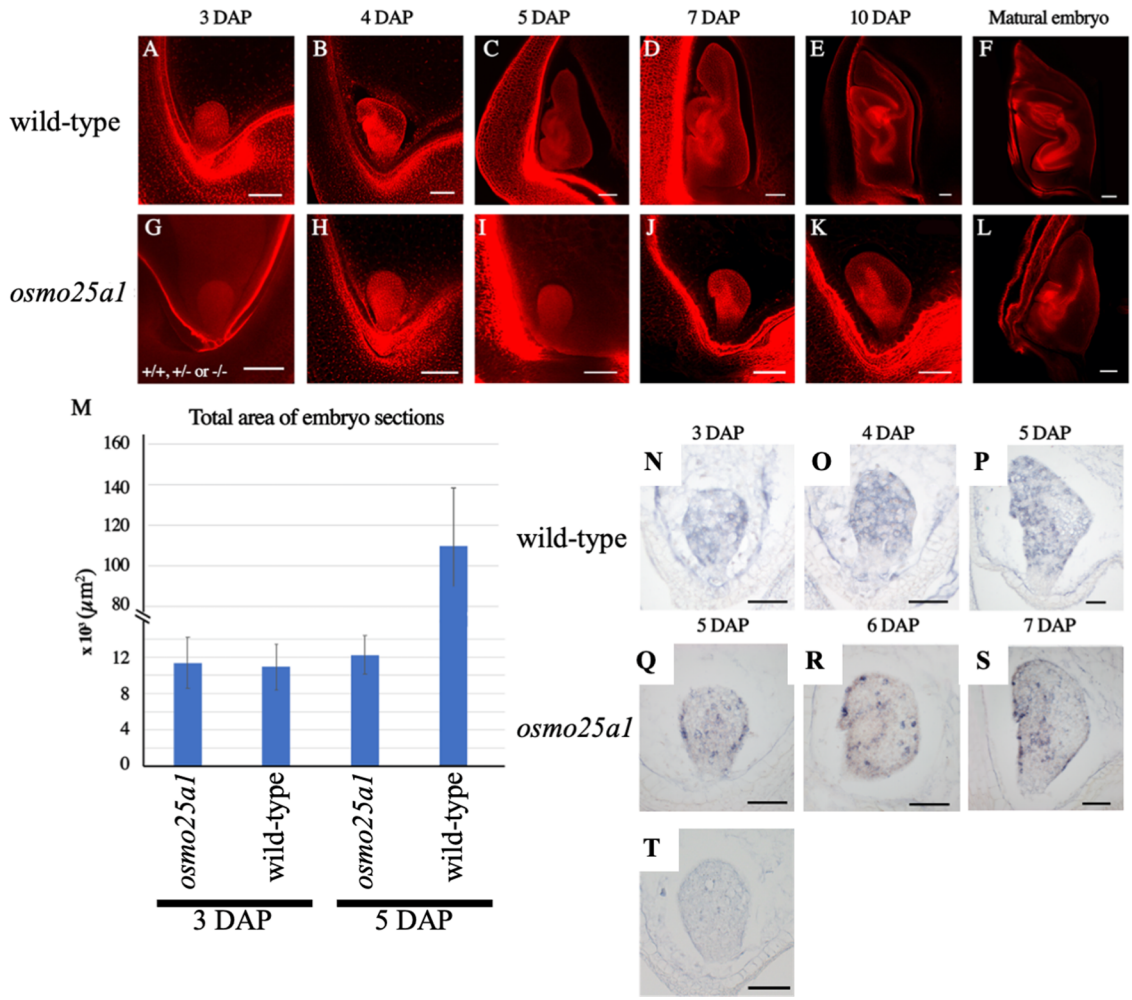

Fig. 2 Delayed embryo development and low mitotic activity in the *osmo25a1* mutant embryo. (A–L) Developmental course of embryo morphology of the WT (A–F) and *osmo25a1* mutant (G–L). At 3 DAP, mutant embryos segregating from heterozygous parents are not distinguished from the WT and heterozygous by morphology; therefore, all three possible genotypes are shown as +/+, ± and −/− in (G). Bars indicate 50 μm. (M) The total area of the sections of WT and *osmo25a1* embryos at 3 and 5 DAP. Error bars indicate standard errors. $N = 3$ (N–T) Mitotic activities of developing embryos of WT (N–P) and *osmo25a1* (Q–S), visualized by in situ mRNA hybridization using a mixture of antisense probes to *HistoneH4* and *Cyclin B*. Control hybridization using a mixture of sense probes to *HistoneH4* and *Cyclin B* is shown in (T). Bars indicate 50 μm.

and third leaf primordia), Em8 at 9 and 10 DAP (enlargement of organs) and mature embryo from dry seed at 40 DAP (Itoh et al. 2005) (**Fig. 2A–L**). The results showed delayed progression of embryogenesis in the *osmo25a1* mutant embryo from 3 DAP. From the zygote stage to 3 DAP, there was no morphological difference between the WT and *osmo25a1* embryos (**Fig. 2A, G**). However, from 3 to 5 DAP, the *osmo25a1* embryo stayed in a globular shape with no discernible growth, whereas in the WT embryo, organogenetic events, including SAM and RAM formation, were prominent during the period (**Fig. 2A–C, G–I**). The size of the mutant embryos at 5 DAP was equivalent to that at 3 DAP in the WT (**Fig. 2M**). At 5 DAP, the mutant embryos appeared to resume organogenetic events, but their growth was much slower than that of the WT (**Fig. 2C, D, I, J**). At 10 DAP, when all organs had formed in the WT embryos, incipient SAM and RAM were barely visible in the *osmo25a1* embryos (**Fig. 2E, K**). In mature embryos, *osmo25a1* formed incomplete organs (**Fig. 2F, L**).

To determine whether the mitotic activity is associated with the delay in *osmo25a1* embryo development, we examined the expression of cell cycle markers (*HistoneH4* and *Cyclin B*) in *osmo25a1* embryos at 5–7 DAP. Even though the morphology of *osmo25a1* mutant embryos at these stages was similar to that of WT embryos at 3–5 DAP, the number of cells expressing the cell cycle markers in *osmo25a1* embryos was much lower than that of a similarly shaped embryo in the WT (**Fig. 2N–T**), and the control hybridization using a mixture of sense probes showed no signal. The expression levels of cell cycle marker genes in WT and mutant cells could not be compared because the signal strength of the in situ hybridization is not always quantitative. Nevertheless, the results indicated that the mitotic activity in the *osmo25a1* mutant embryo is lower than that in

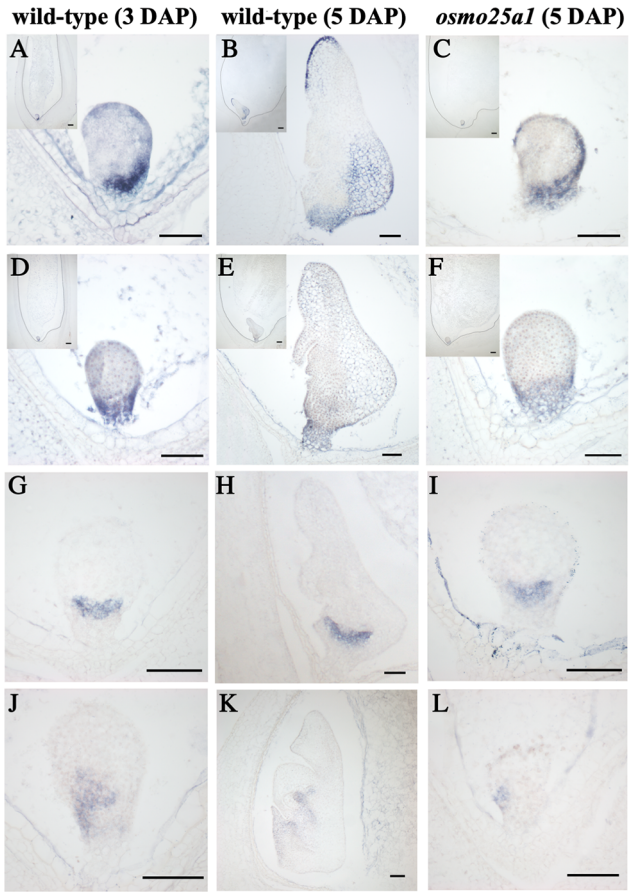

Fig. 3 In situ mRNA hybridization using probes of embryo region–specific marker genes. (A, B, D, E, G, H, J, K) WT embryo at 3 DAP (A, D, G, J) and 5 DAP (B, E, H, K). (C, F, I, L) Mutant embryo at 5 DAP. (A–C) Basal marker Os09g0451000; (D–F) basal marker Os06g0520600; (G–I) root maker Os05g0531200; (J–L) ventral side and shoot maker OSH1. Control hybridization using sense probes showed no signals in all four probes (Itoh et al. 2016, Ishimoto et al. 2019). Bars indicate 50 μm.

the WT, which could cause a delay in embryo development in *osmo25a1*.

Next, we examined the regional specification of the *osmo25a1* mutant embryos at 5 DAP using a set of marker genes that demarcate the regional differentiation in embryos (Itoh et al. 2016, Ishimoto et al. 2019) (**Fig. 3**). Overall, the expression patterns of four marker genes, which demarcate embryonic regions such as apical and dorsal (**Fig. 3A–C**), basal (**Fig. 3D–F**), future radicle (**Fig. 3G–I**) and ventral and future SAM regions (**Fig. 3J–L**) in the mutant embryo at 5 DAP, were indistinguishable from those of the WT at 3 DAP. This indicates that the low mitotic activity in the mutant embryo was not due to the secondary effect of abnormal regional specification.

mRNA expression profiles of *osmo25a1* mutant embryos

To understand the effects of mutation in the *OsMO25A1* gene on mitotic activity in *osmo25a1* embryos, we compared the mRNA profiles of WT and mutant embryos at 3 and 5 DAP (**Fig. 4A, B**). As there was no morphological difference between the WT and mutant embryos at 3 DAP, we confirmed the genotype of each embryo set on heterozygous plants by checking for the mutation in *osmo25a1* mRNA using RNA-sequencing (RNA-seq) data. Clustering analysis showed that the mRNA expression profiles were divided into two clusters, each consisting of embryo samples at 3 and 5 DAP, and WT and mutant embryo samples formed separate groups in each cluster (**Fig. 4A**), which supports the accuracy of the genotypes of each embryo. Next, we extracted differentially expressed genes (DEGs) between all combinations of comparisons of four sets of RNA-seq data, each comprising three to seven biological replicates (**Fig. 4B**). A comparative analysis of mutant and WT embryos at 3 DAP identified 366 DEGs in the mutant embryos with 149 downregulated and 217 upregulated DEGs in the mutants with a false discovery rate (FDR) of <0.05 (**Fig. 4B**), the least difference among the six comparisons, even though in the loosest FDR condition. The result is not surprising because the WT and mutant embryos were morphologically indistinguishable at this stage. In contrast, we observed the largest number of DEGs while comparing WT and mutant embryos at 3 and 5 DAP, respectively, with a total of 4,371 DEGs, of which 2,485 and 1,886 were downregulated and upregulated in the mutants, respectively (FDR < 0.001), even though the WT and mutant embryos were morphologically indistinguishable at 3 and 5 DAP, respectively. Gene ontology (GO) enrichment analysis using DEGs revealed that several genes with GO terms related to metabolic processes, such as primary metabolic processes, were included in both down- and upregulated genes between WT and mutant embryos at 3 and 5 DAP, respectively (**Fig. 4C**). The downregulated DEGs in the mutant between 3 DAP mutant and WT embryos included many GOs and a Kyoto Encyclopedia of Genes and Genomes (KEGG) pathway related to translation, ribosome, ribosomal proteins and peptide synthesis, suggesting an important effect on ribosome biogenesis and protein synthesis in the mutant (**Fig. 4D, E**). Considering that most downregulated DEGs in the mutant embryos at 3 DAP remained downregulated at 5 DAP (**Fig. 4F**), the large differences in RNA expression profiles in mutant embryos at 5 DAP compared to WT embryos at 3 DAP could be caused by reduced protein synthesis at the early stage. In agreement with the observation of reduced mitotic activity in 5 DAP mutant embryos, a comparative analysis of 3 DAP WT and 5 DAP mutant embryos revealed that most cell cycle–related genes were downregulated in the mutant embryos. However, only a few of these genes were downregulated in 3 DAP mutant embryos (**Fig. 4G**).

Expression pattern of *OsMO25A1* in rice

OsMO25A1 is expressed in various tissues and organs, unlike *OsMO25A2*, a paralog of *OsMO25A1* that is expressed in male reproductive organs specifically (**Supplementary Fig. S3**) in agreement with the observation of a mutant phenotype in the embryo

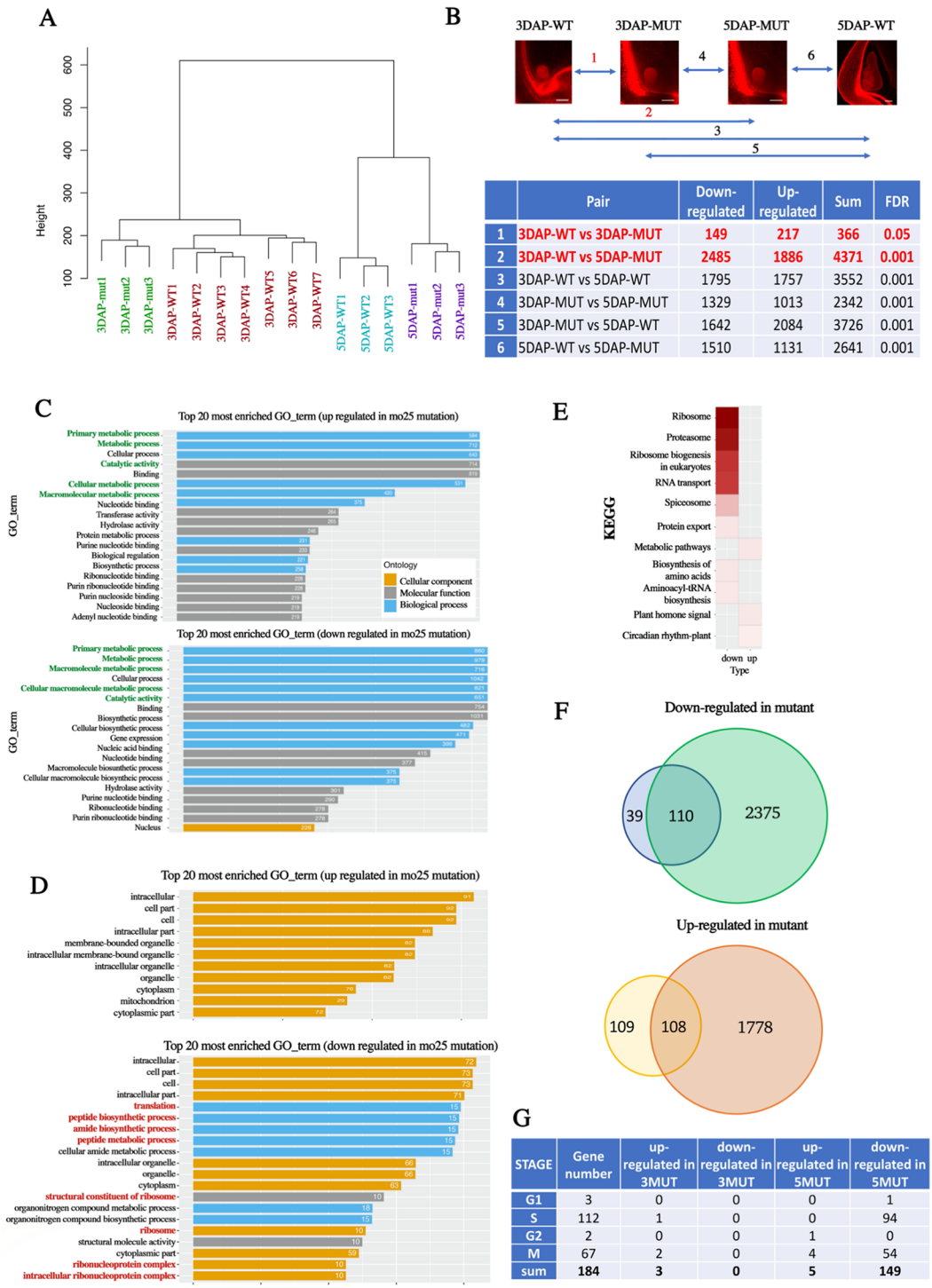

	Pair	Down-regulated	Up-regulated	Sum	FDR
1	3DAP-WT vs 3DAP-MUT	149	217	366	0.05
2	3DAP-WT vs 5DAP-MUT	2485	1886	4371	0.001
3	3DAP-WT vs 5DAP-WT	1795	1757	3552	0.001
4	3DAP-MUT vs 5DAP-MUT	1329	1013	2342	0.001
5	3DAP-MUT vs 5DAP-WT	1642	2084	3726	0.001
6	5DAP-WT vs 5DAP-MUT	1510	1131	2641	0.001

G

STAGE	Gene number	up-regulated in 3MUT	down-regulated in 3MUT	up-regulated in 5MUT	down-regulated in 5MUT
G1	3	0	0	0	1
S	112	1	0	0	94
G2	2	0	0	1	0
M	67	2	0	4	54
sum	**184**	**3**	**0**	**5**	**149**

Fig. 4 mRNA-seq analysis of embryos from *osmo25a1* and WT. (A) Clustering analysis of mRNA expression profiles of embryos from osmo25a and WT at 3 and 5 DAP. (B) A schematic diagram showing all six combinations of mRNA expression profiles of four samples (upper panels) and a summary showing the number of DEGs among all six combinations of comparisons (bottom table). (C) GO terms enrichment analysis using DEGs between mRNA-seq data of 5 DAP mutant embryos and 3 DAP WT embryos. GO terms related to metabolic processes are marked by green characters. The upper and lower panels show GOs enriched in up- and downregulated DEGs, respectively. (D) GO terms enrichment analysis using DEGs between mRNA-seq data of 3 DAP mutant embryos and 3 DAP WT embryos. GO terms related to ribosome and translation are marked by red characters. The upper and lower panels show GOs enriched in up- and downregulated DEGs, respectively. (E) KEGG pathway enrichment analysis using DEGs between mRNA-seq data of 3 DAP mutant embryos and 3 DAP WT embryos. (F) Venn diagrams showing the overlaps of DEGs between mRNA-seq data of 3 DAP mutant and WT embryos, and 5 DAP mutant and 3 DAP WT embryos. The upper and lower diagrams show the overlap of down- and upregulated DEGs, respectively. (G) A summary of the number of cell cycle–related genes, which are expressed at a specific stage of the cell cycle, in DEGs between mRNA-seq data of 3 DAP mutant and WT embryos, and 5 DAP mutant and 3 DAP WT embryos. WT and MUT stand for WT and *osmo25a1*, respectively.

with a single mutation in *OsMO25A1*, despite a close paralog, *OsMO25A2*, in the rice genome. In situ mRNA localization of *OsMO25A1* in young embryos at 3 DAP supports its ubiquitous expression in embryonic cells (**Supplementary Fig. S3**). The accumulation of the OsMO25A1::GFP fusion protein, driven by the *OsMO25A1* promoter, is detectable in the embryos at 3 DAP but not before 3 DAP and is distributed throughout the cytoplasm of scutellum cells in embryos (**Supplementary Fig. S3**). These results strongly suggest that *OsMO25A1* is necessary for the progression of normal embryogenesis after 3 DAP.

Cytoplasmic distribution of MO25A proteins of *P. patens*

To investigate the *in vivo* function of MO25A at the cellular level, we functionally characterized the *MO25A* genes of the moss *P. patens*, a basal land plant, for which genome manipulation and high-resolution live microscopy can be applied easily. Our sequence similarity search identified four genes homologous to *MO25* in *P. patens*, two of which were categorized into the subgroup *MO25A* (Bizotto et al. 2018, **Supplementary Fig. S2**). Hereafter, we refer to them as *PpMO25A1* and *PpMO25A2*, whereas the two *MO25B* genes were designated *PpMO25B1* and *PpMO25B2*. PpMO25A1 and PpMO25A2 were 91% identical in amino acid sequences and had 69% and 55% identity with OsMO25A1, respectively, and 69% and 56% identity with OsMO25A2, respectively. In addition, PpMO25A1 and PpMO25A2 shared 43% and 44% identity with human MO25α, respectively, and 46% and 47% identity with human MO25β, respectively.

We first determined the subcellular localizations of PpMO25A1 and PpMO25A2 in living cells. To this end, we fused mNeonGreen (mNG) to the C-terminus via homologous recombination. The fluorescence intensity indicated that PpMO25A1 was more abundant than PpMO25A2 (**Fig. 5A**). Both proteins were distributed throughout the cytoplasm of protonemal apical stem cells without particular enrichment at the cell tip or cell plate, which differed from their fungal counterparts (**Fig. 5A**).

Loss-of-function mutants of the *PpMO25A* gene showed developmental defects

Next, we attempted to establish a complete knockout (KO) mutant of *MO25A* in which both *PpMO25A1* and *PpMO25A2* were deleted by homologous recombination. As depicted in **Supplementary Fig. S4A**, plasmids targeting each *PpMO25A* gene were constructed and sequentially transformed into mosses. We successfully obtained single KO lines. The growth patterns of *PpMO25A1* or *PpMO25A2* single KO lines were not drastically different from those of the control (**Fig. 5B**, **Supplementary Fig. S5A**). However, the *PpMO25A2* gene could not be deleted in the background of *PpMO25A1* KO after multiple transformation attempts. These results suggest that these two genes act redundantly, but neither one is necessary for moss viability.

Next, we attempted to obtain hypomorphic mutants of *MO25A* by deleting part of the coding region of *PpMO25A2* using CRISPR/Cas9 technology (Lopez-Obando et al. 2016, Collonnier et al. 2017). We transformed multiple guide RNA sequences targeting the middle or posterior region of *PpMO25A2* into the *PpMO25A1* KO line (**Supplementary Fig. S4B**). Consequently, we obtained several mutants that grew poorly compared to the parental *PpMO25A1* KO line in which partial deletions within *PpMO25A2* were confirmed by sequencing (**Supplementary Fig. S4C**). One allele, designated as *Ppmo25a1a2-1*, had a 5-bp deletion at nucleotide (nt.) 974–978, causing a frameshift in the amino acid sequences. The other allele, *Ppmo25a1a2-2*, had a 3-bp deletion at nt. 308–310, which produces the PpMO25A2 protein lacking the Leu103 residue.

To quantitatively assess the growth phenotype, protoplasts of the mutants were isolated and regrown on an agar medium. The *Ppmo25a1a2-1* and *Ppmo25a1a2-2* mutants revealed drastic and moderate growth suppression, respectively (**Fig. 5B, C**). *Physcomitrium patens* protonemata consist of chloronemal and caulonemal cells, distinguishable by the shape and color of the chloroplasts (Kofuji and Hasebe 2014). However, caulonemal cells predominated as the apical cells of the protonemal filaments in the *Ppmo25a1a2-1* mutant. Time-lapse microscopy indicated that the rate of tip growth of the caulonemal apical cells decreased, explaining the difference in plant size (**Fig. 5D**). Furthermore, gametophores were small (**Fig. 5B**, bottom) and developed at a considerably low frequency (**Fig. 5B**, **Supplementary Fig. S5B**) in *Ppmo25a1a2-1*. These phenotypes were significantly, if not completely, suppressed by the expression of MO25A2-mNG from a non-native locus with a non-native promoter in the mutants (**Fig. 5B**, **Supplementary Fig. S5B**). We concluded that *PpMO25A2* is required for the proper development of protonemata and gametophores in the absence of *PpMO25A1*.

Tip growth of protonemal branch cells is suppressed in the *Ppmo25a* mutants

We applied high-resolution live confocal microscopy to the *Ppmo25a1a2-1* mutants to identify cellular phenotypes. The mitotic progression appeared normal (**Supplementary Movie**). The most prominent phenotype in protonemata was the suppression of branching filament growth (**Fig. 6A, B**). In the control protonemata, branch filaments are formed following sequential events in the subapical cell: (i) bulge formation, (ii) nuclear division and cytokinesis and (iii) tip growth (Yi and Goshima 2020). In the mutants, the first two events occurred as in the control, as evidenced by the formation of branch cells with the nucleus and cell plate (**Fig. 6B**; circles and arrowheads). However, similar to apical cells of the main filament, the newly produced branch cells grew extremely slowly compared to the control line (1.7 ± 0.5 in the control vs. 0.3 ± 0.1 μm/h

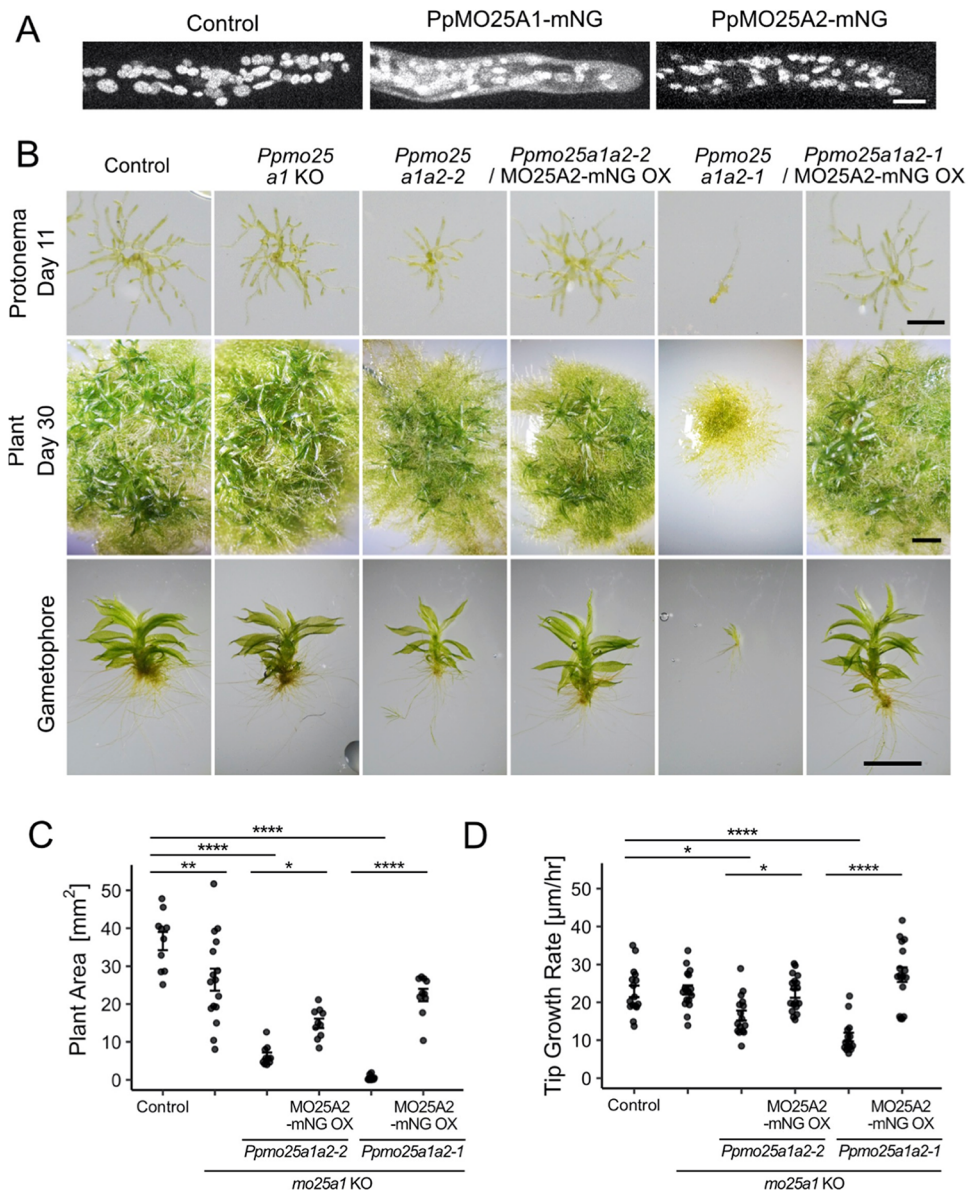

Fig. 5 Developmental defects of the *Ppmo25a1a2* mutants. (A) Localization of PpMO25A1 and PpMO25A2 in protonemal apical cells. Note that ellipsoidal signals are due to chloroplast autofluorescence, observed also in an mNG-untagged line (left). Scale bar, 10 μm. (B) Observation of the moss growing from a single protoplast. First row: protonemal cells regenerating from protoplasts cultured for 11 d. Scale bar, 200 μm. Second row: plant surface on day 30. Scale bar, 2 mm. Third row: gametophore morphology. Each gametophore was picked up from the plate on day 30. Scale bar, 2 mm. (C) Quantification of plant area incubated 30 d from single protoplast stage. OX stands for overexpression. The mean area (mm^2) is 36.6 ± 2.40 (control; ±SEM, $n = 10$), 26.4 ± 2.92 (*mo25a1* KO; ±SEM, $n = 16$), 6.35 ± 0.838 (*Ppmo25a1a2-2*; ±SEM, $n = 10$), 14.9 ± 1.24 (MO25A2-mNG OX/*Ppmo25a1a2-2*; ±SEM, $n = 10$), 0.553 ± 0.222 (*Ppmo25a1a2-1*; ±SEM, $n = 10$) and 22.4 ± 1.64 (MO25A2-mNG OX/*Ppmo25a1a2-1*; ±SEM, $n = 10$). (D) Tip growth rate of protonemal cells quantified from data acquired with long-term live imaging. The mean rate (μm/h) is 22.9 ± 1.53 (control; ± SEM, $n = 16$), 23.2 ± 1.22 (*mo25a1* KO; ± SEM, $n = 17$), 16.5 ± 1.31 (*Ppmo25a1a2-2*; ± SEM, $n = 16$), 22.3 ± 1.11 (MO25A2-mNG OX/*Ppmo25a1a2-2*; ± SEM, $n = 18$), 10.8 ± 1.12 (*Ppmo25a1a2-1*; ± SEM, $n = 15$) and 27.3 ± 1.95 (MO25A2-mNG OX/*Ppmo25a1a2-1*; ± SEM, $n = 17$).

in *Ppmo25a1a2-1*: **Fig. 6B, C**). Ectopic expression of full-length PpMO25A2-mNG restored the growth rate, indicating that the phenotype was derived from PpMO25A2 dysfunction in the mutant. We concluded that PpMO25A promotes the tip growth of branch cells in protonemata.

Gametophore induction is suppressed in the *Ppmo25a1a2-1* mutants

As *Ppmo25a1a2-1* showed a significant reduction in the number of mature gametophores, we hypothesized that MO25A is required to initiate gametophore development. In *P. patens*,

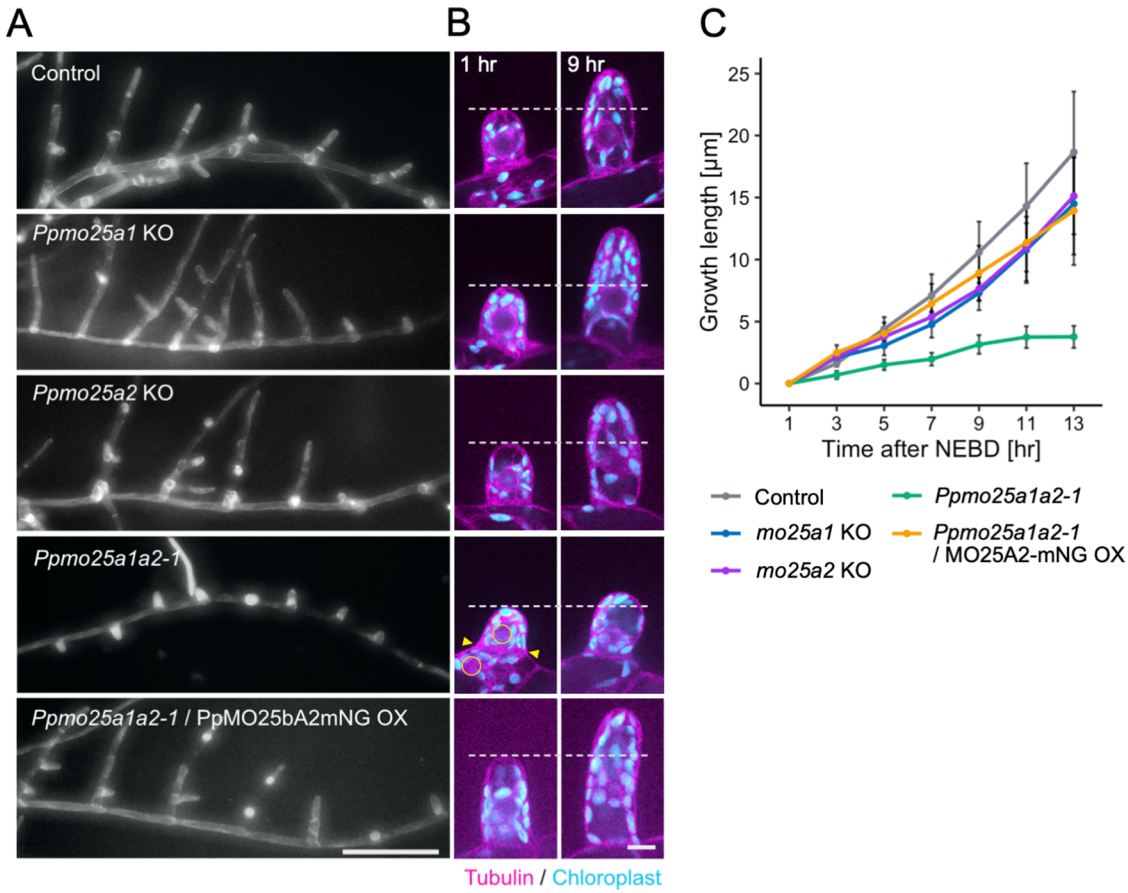

Fig. 6 Growth of protonemal branch cells was suppressed in *Ppmo25a1a2-1*. (A) Protonemal filaments with branches of each line are presented. Scale bar, 200 μm. (B) Branch cells at 1 h (left) and 9 h (right) after NEBD. Yellow circles and arrowheads indicate the position of nuclei and the cell wall, respectively. Scale bar, 10 μm. (C) Branch cell length over time. Error bars represent ±SEM; $N = 6$ cells for each strain and OX stands for overexpression.

the gametophore initially emerges as a bud, mainly from the caulonemal cells (Bopp 1963). Branch cells and buds are distinguishable by their morphology and the location of the cell plate (Kofuji and Hasebe 2014, Tang et al. 2020). In the control cells, the bud was observed at a similar frequency to previous studies (5.5%, $n = 10$ plants) (Cove and Knight 1993). In contrast, the frequency was much lower in the *Ppmo25a1a2-1* mutants (1.0%, $n = 10$). The frequency was increased by expressing PpMO25A2-mNG (6.8%, $n = 10$). Thus, the initiation of gametophore formation was perturbed in the mutant. In moss, bud formation requires cytokinin. Furthermore, exogenous cytokinin treatment promotes bud formation (Hahn and Bopp 1968, Beutelmann and Bauer 1977, Reski and Abel 1985). When the native cytokinin isopentenyladenine (2iP) was added to the culture medium, the *Ppmo25a1a2-1* mutant produced many gametophore buds (**Fig. 7A**). Thus, the mutants responded to exogenous cytokinins, suggesting that PpMO25A is involved in the biosynthesis of cytokinins and/or a shift in signaling sensitivity.

Accelerated cell growth and delayed mitotic entry in gametophore initials of the *Ppmo25a1a2-1* mutant

Next, we observed the growth and division of the gametophore initial induced by 2iP using live-cell imaging (**Fig. 7B, C**). In the control line expressing mCherry-tubulin, the gametophore initial cell emerged via bud tip growth, and the first prometaphase began with nuclear envelope breakdown (NEBD) at 28 ± 1.3 h ($n = 14$) after 2iP treatment (**Fig. 7D**). The bud tip growth rate was 2.2 ± 0.26 μm/h (±SEM, $n = 8$) (**Fig. 7E**). In the *Ppmo25a1a2-1* mutant, the first NEBD was delayed by several hours (36 ± 1.4 h, $n = 20$). Surprisingly, the growth rate of the bud tip was faster in the mutants than in the control lines, contrary to the case of branch tips (**Fig. 7E**). Consequently, the cell at the time of the first NEBD was significantly longer in the mutant (74 ± 4.8 μm, $n = 8$) than in the control (52 ± 1.7 μm, $n = 8$, **Fig. 7F**). The initiation of the second and third divisions of the gametophore initial was also delayed in the *Ppmo25a1a2-1* mutant, particularly for the basal

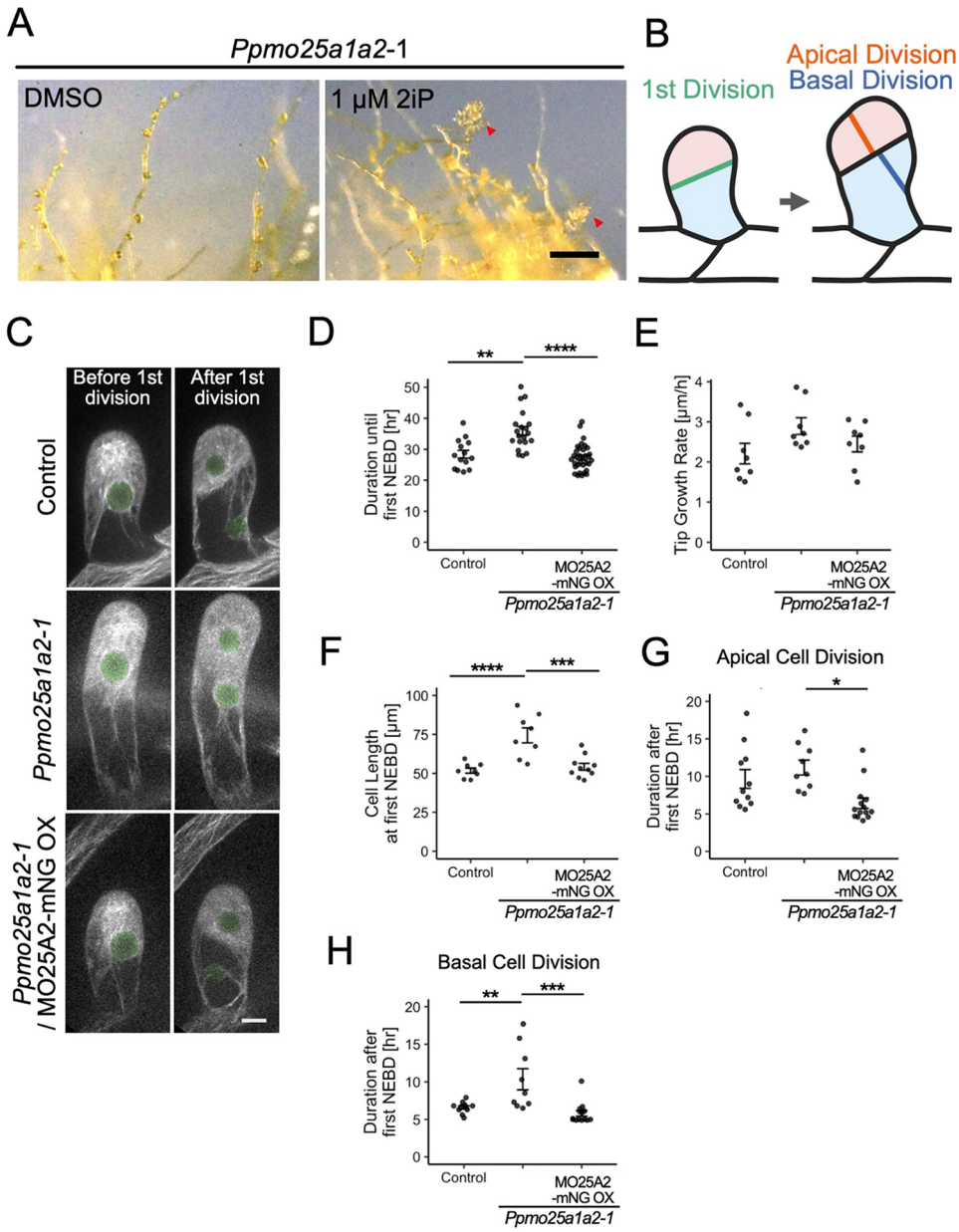

Fig. 7 Induced gametophore of *Ppmo25a1a2-1* showed an increase in the tip growth rate and a delay in division initiation. (A) Gametophore initiation in *Ppmo25a1a2-1* incubated in BCDAT media containing 1 μM 2iP (control; DMSO alone added). Red arrowheads indicate gametophore buds. Scale bar, 500 μm. (B) Cell growth and division in the gametophore initial of *P. patens*. (C) Induced gametophore initial cells before and after the first cell division. The left column presents the cells just before NEBD of the first division. The right column presents the cells that completed cytokinesis. The nuclear position is indicated by green. Scale bar, 10 μm. (D) Quantification of duration from the addition of 2iP to NEBD of the first cell division of induced gametophore initial cells. The mean duration (h) is 28.4 ± 1.27 (control; ±SEM, $n = 14$), 36.0 ± 1.41 (*Ppmo25a1a2-1*; ±SEM, $n = 20$) and 27.3 ± 0.744 (MO25A2-mNG OX/*Ppmo25a1a2-1*; ±SEM, $n = 33$). (E) Quantification of the tip growth rate of induced gametophore initial cells. The mean rate (μm/h) is 2.21 ± 0.258 (control; ±SEM, $n = 8$), 2.90 ± 0.207 (*Ppmo25a1a2-1*; ±SEM, $n = 8$) and 2.45 ± 0.198 (MO25A2-mNG OX/*Ppmo25a1a2-1*; ±SEM, $n = 8$). (F) Quantification of cell length at the time of NEBD of the first cell division of induced gametophore initial cells. The mean length (μm) is 51.8 ± 1.68 (control; ±SEM, $n = 8$), 75.4 ± 4.82 (*Ppmo25a1a2-1*; ±SEM, $n = 8$) and 54.2 ± 2.20 (MO25A2-mNG OX/*Ppmo25a1a2-1*; ±SEM, $n = 10$). (G) Quantification of duration between NEBD events of the first and second mitoses in the apical cell of the gametophore initial. The mean duration (h) is 9.66 ± 1.26 (control; ±SEM, $n = 11$), 11.2 ± 0.996 (*Ppmo25a1a2-1*; ±SEM, $n = 9$) and 6.44 ± 0.705 (MO25A2-mNG OX/*Ppmo25a1a2-1*; ±SEM, $n = 14$). (H) Quantification of duration between NEBD events of the first and second mitoses in the basal cell of the gametophore initial. The mean duration (h) is 6.58 ± 0.224 (control; ±SEM, $n = 11$), 10.3 ± 1.40 (*Ppmo25a1a2-1*; ±SEM, $n = 9$) and 5.79 ± 0.373 (MO25A2-mNG OX/*Ppmo25a1a2-1*; ±SEM, $n = 14$).

cell, suggesting a longer cell cycle duration in the absence of functional PpMO25A2 in the gametophore initial (**Fig. 7G, H**). These values were restored to nearly the control levels when PpMO25A2-mNG was expressed ectopically in the mutants. These results indicate that PpMO25A regulates cell growth and cell cycle in the gametophore initial. Notably, the regulation of cell growth in gametophore initials was different from that in protonemal tissues, suggesting the versatile roles of MO25 during moss development.

Discussion

In this study, we identified *OsMO25A1*, which belongs to a family of genes encoding MO25A, as the causative gene for a mutation that significantly delays the progression of rice embryogenesis and is associated with the reduced mitotic activity. From the analysis of the rice *osmo25a1* mutation, we found that *OsMO25A1* was important for maintaining mitotic activity in the embryos beyond 3 DAP. We also found that *PpMO25A1* and *PpMO25A2*, members of the MO25A family of *P. patens*, were critical for moss growth and development. The hypomorphic mutants showed abnormalities in the protonema branch and gametophore initials, where the apical cells represent stem cells (Kofuji and Hasebe 2014). In the protonema branch, cell tip growth was suppressed, whereas, in gametophore initials, cell cycle abnormalities associated with delayed NEBD were prominent. Thus, plant MO25A proteins are involved in multiple cell growth and division stages.

Notably, the phenotypes caused by the reduced activity of MO25A in moss seem to differ depending on the cell type. For example, the tip growth of the gametophore initial cell was enhanced, whereas the tip growth of the protonemal branch cell was suppressed in the *Ppmo25a1a2*, suggesting that PpMO25A proteins are not general components that execute cellular activities such as tip growth. Rather, these could mediate a signal that regulates cellular activities in a cell type–specific manner. The reduced mitotic activity observed in the *osmo25a1* mutants also supports the idea because, in the *osmo25a1* mutant embryos, cell proliferation continues at a reduced rate. Thus, we propose that plant MO25A proteins execute the cell type–specific characteristics of cell growth and proliferation responsible for intrinsic developmental signals.

MO25 proteins function as kinase scaffolds operating in a widely conserved signaling pathway, the Hippo/MST kinase pathway, also known as the MOR pathway, in metazoans and fungi. These kinases belong to a highly conserved subclass of (AGC) protein kinases, one of the six kinase families conserved in all eukaryotes (Miranda-Saavedra and Barton 2007). In the *Arabidopsis* genome, there are 39 genes encoding AGC kinases, which are expected to function in various cellular and developmental processes. Many plant AGC kinases have orthologous genes in mammals, including the NDR kinase subfamily; thus, these could be candidate pathways in which plant MO25 functions. Nine AGC kinase families, including PINOID, WAG1, WAG2 and D6PK, regulate auxin transport (Rademacher and Offringa 2012). Although they belong to plant-specific subgroups of the AGC kinase family, it is intriguing to speculate that plant MO25 is involved in auxin transport regulation.

In *Saccharomyces cerevisiae*, mutations in *Cdc15*, which belongs to the MST family of kinases, result in abnormalities in the mitotic exit network (MEN) and cause cell cycle arrest at late mitosis (Pringle and Hartwell 1981, Surana et al. 1993, Jaspersen et al. 1998). Although the defective cell proliferation phenotypes observed in mutants of MO25A genes in rice and moss are not typical MEN abnormalities, it is noteworthy that in both rice and moss, mutations in genes encoding MO25A showed phenotypes related to cell proliferation. The function of the MO25A gene in plants has not been reported previously, and this study is the first to demonstrate the importance of plant MO25A in cell proliferation. Thus, this study suggests that MO25A is a widely conserved regulator of signaling involved in eukaryotic cell proliferation.

In mammals and budding yeast, the MO25 protein is involved in cell polarity and tip growth. The suppression of protonema branch tip growth in *PpMO25A* mutants may also reflect a conserved function of the MO25 family. Because the rice *osmo25a1* mutation is embryonically lethal, we do not know the function of *OsMO25A1* at sites where tip growth is prominent. In contrast, the subcellular localization of MO25A in plants is markedly different from that of MO25 in mammals and yeast. Although in mammals and fungi, MO25 has been proposed to localize to specific regions of the plasma membrane or to the site of cell division to anchor MST kinases (Mendoza et al. 2005, Goshima et al. 2010, Filippi et al. 2011, Dettmann et al. 2012), both PpMO25A1 and PpMO25A2 appear to be distributed uniformly in the cytoplasm. Similarly, localization to the plasma membrane or specific organelles could not be observed in OsMO25A1. The kinases interacting with plant MO25A and the mechanism of their regulation by MO25A in the cytoplasm remain to be determined.

osmo25a1 mutant embryos were morphologically indistinguishable from WT embryos up to 3 DAP. *osmo25a1* mutation is located at a splice donor site, and there is an insertion or deletion mutation in CRISPR lines, suggesting that these are all null alleles. All these mutations resulted in similar embryo phenotypes, implying that the OsMO25A1 function is not required until 3 DAP but only beyond 3 DAP. Indeed, the fluorescence of the OsMO25A1::GFP fusion protein expressed under the *OsMO25A1* promoter was observed at 3 DAP. Interestingly, cells proliferate normally until 3 DAP without functional OsMO25A1 in rice mutants, despite the conserved and pivotal function of MO25A in cell proliferation. *OsMO25A2*, a paralogous gene with high sequence similarity to *OsMO25A1*, is strongly expressed in mature anthers but not in other saprophytic tissues and organs (**Supplementary Fig. S3**). *OsMO25A2* expression was detected in the sperm cells of pollens using RNA expression data (Rahman et al. 2019). If sperm cell–derived OsMO25A2 is involved in cell proliferation after fertilization until 3 DAP, when OsMO25A1 begins to accumulate, this could be an interesting mechanism to ensure the onset of sporophytic development after fertilization by supplying pollen-derived MO25A.

Embryogenesis is a process in which cell proliferation and differentiation are coordinately regulated (ten Hove et al. 2015). *osmo25a1* mutants showed reduced expression of most cell cycle–related genes beyond 3 DAP. However, there were no abnormalities in the region-specific differentiation of *osmo25a1* mutant embryos, implying that embryonic regional specification is completed at 3 DAP in mutants and WTs. Even though the expression of embryonic regional markers in 5 DAP mutant embryos was similar to that of morphologically indistinguishable WT 3 DAP, the profiles of mRNA expression revealed that there exists the largest number of DEGs in comparison with 5 DAP mutant and 3 DAP WT embryos. These DEGs included many genes implicated in primary metabolism, suggesting that OsMO25A1 affects basic cellular activity rather than being involved in regional or cellular specification during embryogenesis, in reasonable agreement with the reduced mitotic activity in the mutant embryos.

On the other hand, only a small number of DEGs could be observed between the WT and mutant embryos at 3 DAP. These included many genes involved in ribosomal translation. Downstream factors of the Hippo pathway in *Drosophila* are involved in ribosome biosynthesis and cell proliferation (Neto-Silva et al. 2010, Ziosi et al. 2010), suggesting a multifaceted role for MO25 in plants and animals, despite the possibility that ribosome biosynthesis, cell proliferation and the speed of development are interconnected, as evident in *Minute* mutations in *Drosophila* (Bridges and Morgan 1923, Marygold et al. 2007).

Cell growth and proliferation are fundamental processes that support the development of multicellular organisms and are regulated in various ways to define the size of individuals and organs. Indeed, the size of individuals and their organs is modulated by altering the frequency of cell division (reviewed in Jakoby and Schnittger 2004, de Jager et al. 2005). The size of individuals and organs is subject to highly complex regulation in response to physiological cues such as the availability of nutrients. However, intrinsic developmental signaling that leads to cell growth and proliferation is less explored in plants. The Hippo/MST kinase pathway is a key regulator of organ size in mammals and *Drosophila* (Pan 2010, Zhao et al. 2011). This study is the first step toward elucidating signaling mediated by MO25 and possibly the Hippo/MST kinase pathway in plants.

Materials and Methods

Plant materials and growth conditions

Screening of chemically mutagenized populations of *Oryza sativa* strain T-65 yielded *08T6S44* seeds. *08T6S44* and Taichung 65 seedlings were grown in a paddy field under normal conditions to obtain samples for histological observation, in situ hybridization and transcriptome analyses. Transgenic plants were grown in a controlled growth chamber, as described by Ohnishi et al. (2011). All *P. patens* strains in this study were derived from the Gransden ecotype of *P.* (*Physcomitrella*) *patens* (Ashton and Cove 1977). *Physcomitrium patens* was cultured on BCDAT plates at 25°C under continuous light illumination (Yamada et al. 2016).

Genotyping of *08T6S44* mutants

The *08T6S44* genotypes were determined by sequencing the PCR products using the following primer sets: *08T6S44*_genotyping_F1:5′-CGGCGGGACCAGTGGCGCTG-3′ and *08T6S44*_genotyping_R1:5′-GTTACATCAAATTGAAGGAACAGAG-3′. PCR was conducted using GoTaq Green Master Mix (Promega), following the manufacturer's instructions.

Production of transgenic plants

For the molecular complementation test, 3.0 kb of the promoter region and 1,008 bp of the coding sequence (CDS) were incorporated into the pGWB1 vector using an In-Fusion HD Cloning Kit (Takara, Shiga, Japan). The promoter and CDS regions were amplified using the following primer sets: *OsMO25p*_F1, 5′-GGAAGCTTGAGAGCCGACAAAGTTTGG-3′; *OsMO25p*_R1, 5′-GAAGAGGCCCTTCATCTTGGCGCCGTCGTC-3′; *OsMO25cds*_F1, 5′-ATGAAGGGCCTCTTCAAGTCCAAGCCGCGG-3′, and *OsMO25cds*_R1, 5′-TGCTCACCATGCCACCGCCAAGTGCAGAT-3′. The resulting plasmids were introduced into *Agrobacterium tumefaciens* EHA105 and then used to transform the *osmo25a1*/+ heterozygous rice calli (Hiei et al. 1994), and we selected the plants carrying the transgene in the heterozygous mutant background. Regenerated plants were grown in a growth chamber, as described earlier, to obtain self-pollinated seeds. After germination, we genotyped each seedling and obtained *osmo25a1* homozygous plants and seed sets from these plants.

The *OsMO25* CRISPR/Cas9 vector was constructed using the method described by Mikami et al. (2015) to produce genome-edited plants. The target sequence of *OsMO25* was 5′-AAGTTGTTGCAAACTTGCAA-3′ (sense strand). For genome editing, DNA fragments were amplified using the primer sets (*08T6S44*_genotyping_F1 and *08T6S44*_genotyping_R1) and sequenced. *Physcomitrium patens* transformation was performed as described previously (Yamada et al. 2016, Yoshida et al. 2022). The transformation was performed using the standard polyethylene glycol–mediated method. Before the transformation, sonicated protonemata were cultured on BCDAT agar for 5–6 d. Transgenic lines were selected using the corresponding antibiotics. Line confirmation was conducted by genotyping through PCR and visual inspection (**Supplementary Fig. S6**). Sequencing was performed to confirm the CRISPR mutant lines. The lines generated in this study are listed in **Supplementary Table S1**. The plasmids and primers used for *P. patens* are listed in **Supplementary Tables S2 and S3**, respectively. The 1–2-kb sequences of the 5′ and 3′ UTR of *PpMO25A1* were amplified from gDNA and flanked by the G418 resistance cassette in the background of pENTR/D-TOPO using the In-Fusion HD Cloning Kit (Takara) to establish KO moss by homologous recombination. CRISPR targets of *PpMO25A2* with high specificity were manually selected within the *PpMO25A2* coding region, as described in **Supplementary Fig. S4B**. All target sequences were synthesized and ligated into the *Bsa*I site of pPY156, which is based on pCasGuide/pUC18 and contains a hygromycin-resistance cassette (Collonnier et al. 2017). In addition, the plasmid was constructed using the In-Fusion HD Cloning Kit (Takara) for endogenous tagging via homologous recombination. The 1–2-kb sequences of the 5′ and 3′ ends of the genes of interest flanked the fragment that consisted of an in-frame linker, an mNG CDS, a Flag tag and a hygromycin-resistance cassette. The mNG codon has been optimized for expression in *Arabidopsis*. For the rescue experiment, the *MO25A2* CDS was amplified from the moss cDNA library and ligated into the pENTR/D-TOPO vector containing the in-frame linker, mNG CDS and Flag tag, followed by the Gateway LR reaction (Invitrogen, Waltham, MA, USA) into the pPY185 vector containing the *EF1α* promoter, Nourseothricin (NTC) resistance cassette and 1-kb sequences homologous to the *hb7* locus.

Phenotypic observation of rice mutants

Mature seeds were cut in half through the center of the embryo, and pistils containing embryos at 3–10 DAP were fixed in a 1:1:18 solution of 37% formaldehyde, acetic acid and ethanol under vacuum two times for 1 h each and then overnight at 4°C. After gradually replacing ethanol with 1× PBS buffer, samples

were stained with 5.0 μg/ml propidium iodide solution (Dojindo, Kumamoto, Japan) containing 10.0 μg/ml RNase A (Invitrogen) in 1× PBS buffer overnight in the dark at 4°C. After dehydration in a graded ethanol series, ethanol was replaced with methyl salicylate for transparency. Propidium iodide fluorescence emission at 570–670 nm (excitation at 559 nm) was captured using a confocal laser scanning microscope (FV3000, Olympus, Shinjyuku, Tokyo, Japan).

In situ hybridization

Full-length cDNA fragments were amplified with the following primer sets: *OsMO25atg*_F1, 5′-ATGAAGGGCCTCTTCAAGTCCAAG-3′; *OsMO25-stop*_R1, 5′-CTAAAGTGCAGATATCTCCTTTATGAC-3′; *HistoneH4atg*_F1, 5′-ATGTCTGGGAGAGGCAAGGGCGGC-3′; *HistoneH4stop*_R1, 5′-CTAGCCGCC-GAATCCGTAGAGGGT-3′; *cyclin Batg*_F1, 5′-ATGGAGAACATGAGATCTGAG-AAC-3′, and *cyclin Bstop*_R1, 5′-TTACAGTGCCACGCTCTTGAGCAA-3′, using total RNA prepared from roots to prepare digoxigenin-labeled *OsMO25A1*, *HistoneH4* and *Cyclin B* probes. Sense and antisense probes were synthesized using the MAXIscript T7/T3 Transcription Kit (Thermo Fisher Scientific, Waltham, MA, USA) with digoxigenin-11-UTP (Roche, Basel, Kanton, Switzerland). Other cDNA probes were prepared as previously described (Itoh et al. 2016).

For in situ hybridization, ovaries containing embryos at 3–7 DAP were fixed in a 2:1:10:7 solution of 37% formaldehyde, acetic acid, ethanol and water under vacuum two times for 1 h each and then overnight at 4°C. The samples were dehydrated using a graded ethanol series. Ethanol was replaced with Histo-Clear II (National Diagnostics, Atlanta, GA, USA), and the samples were embedded in Paraplast Plus (Leica, Wetlar, Hessen, Germany). Sections of 8-μm thickness were cut using a rotary microtome and mounted on microscope slides coated with 3-aminopropyl triethoxysilane (Matsunami Glass, Kishiwada, Osaka, Japan). In situ hybridization was performed as previously described (Kouchi and Hata 1993). Hybridization was conducted overnight at 52°C, and coloring was conducted overnight at 30°C.

Laser microdissection

Ovaries of *08T6S44* heterozygous plants were fixed at 3 and 5 DAP in a pre-chilled solution of 75% ethanol:25% acetic acid with vacuum infiltration. After dehydration in a graded ethanol series, the tissues were embedded in Paraplast X-tra (Leica) using a microwave processor (Energy Beam Sciences, East Granby, CT, USA), according to Takahashi et al. (2010). Sections (16 μm thick) were cut with a rotary microtome and applied onto poly ethylene napthalate membrane glass slides (Leica). Laser microdissection was performed using an LMD6000 Laser Microdissection System (Leica). Total RNA extraction was performed as previously described (Ishimoto et al. 2019).

Transcriptome analysis of rice embryos

RNA samples were converted into cDNA using the SMART-Seq HT Kit (Clontech, Kusatsu, Shiga, Japan) following the manufacturer's instructions. After converting cDNA, sequencing libraries were constructed using the Nextera XT DNA library Prep Kit and IDT for Illumina Nextera DNA Unique Dual Index (Illumina, San Diego, CA, USA) and purified with Agencourt AMPure XP (Beckman, Brea, CA, USA). Sequencing was performed using the Illumina NovaSeq6000 platform, and the resulting reads were mapped to the reference genome of *O. sativa* (IRGSP 1.0) using RAP-DB annotations with STAR (Dobin et al. 2013). The 'quantMode' argument in STAR was used for counting the reads. Transcript expression was evaluated using the EdgeR package in R (Robinson et al. 2010), and transcript abundance was estimated using counts per million mapped fragments. DEGs were selected using FDR with $P < 0.001$ or $P < 0.05$ and a fold change value of >2. DEGs were analyzed using annotations from the MSUv7, RAP-DB and Oryzabase databases. GO analysis was conducted using AgriGO (http://bioinfo.cau.edu.cn/agriGO/) and g:Profiler (https://biit.cs.ut.ee/gprofiler/). All plots were generated using the *ggplot2* R package.

Microscopy

Subcellular localization of OsMO25A1 fused to GFP was observed after tissue clearing using the standard iTOMEI method (Sakamoto et al. 2022) with a confocal laser scanning microscope (FV3000, Olympus). Time-lapse microscopy was performed as described previously (Nakaoka et al. 2012, Yoshida et al. 2022). Briefly, in long-term time-lapse imaging experiments to observe protonemal cells, protonemata were cultured on thin layers of BCD agarose in six-well glass-bottom dishes for 5–7 d. Epifluorescence images were acquired using a (Nikon, Minato, Tokyo, Japan) Ti microscope (10× 0.45 NA lens, Zyla 4.2P CMOS camera, (Andor, Belfast, Northern Ireland, UK); Nikon Intensilight Epi-fluorescence Illuminator) at intervals of 3–10 min with white light between acquisitions. For high-resolution imaging, protonemata were inoculated onto the agar pad in a 35-mm glass-bottom dish, followed by culturing for 5–7 d. Confocal imaging was performed with a Nikon Ti microscope attached to a CSU-X1 spinning disk confocal scanner unit (Yokogawa, Musashino, Tokyo, Japan), an EMCCD camera (ImagEM, Hamamatsu Photonics, Hamamatsu, Shizuoka, Japan) and three laser lines (637, 561 and 488 nm). Lenses were selected depending on the experiment (60× 1.40 NA and 100× 1.45 NA). Twenty hours before confocal imaging, 1.0 μM 2iP (Nacalai Tesque, Nakagyo, Kyoto, Japan) was added to 4- to 5-day-old protonemata on sample dishes to induce gametophore initial cells. Most imaging was performed at 22–25°C in the dark, except for the data used to obtain the tip growth rate shown in **Fig. 6C**, which were obtained under continuous light.

Moss growth assay

The method described by Yoshida et al. (2022) was used. The 5- to 7-day-old sonicated protonemata were digested using an 8% (w/v) mannitol solution supplemented with 1% (w/v) driselase for 0.5–1 h to prepare the protoplasts. After removing the driselase by washing twice with an 8% mannitol solution, the protoplasts were resuspended in the protoplast regeneration liquid (Vidali et al. 2007). After 4 h of incubation in the dark, protoplasts were collected by centrifugation, resuspended in 7.5 ml of protoplast regeneration media (PRM) solution (Yamada et al. 2016) and spread onto three PRM plates covered with cellophane. The protoplasts were cultured for 3 d and transferred to a BCDAT plate. Images of 7-day-old moss protonemata were captured using a stereomicroscope SMZ800N (Nikon) equipped with an ILCE-QX1 camera (SONY, Minato, Tokyo, Japan). The 9-day-old protonemata were inoculated onto BCDAT plates and cultured for 3–5 weeks. Images of all plants or gametophores were captured using a C-765 Ultra Zoom digital camera (Olympus) or SMZ800N and ILCE-QX1, respectively. Twenty-five hours before observation, 1.0 μM 2iP was added to protonemata on sample dishes to assess gametophore induction ability. Images were acquired using the SMZ800N and ILCE-QX1.

Moss image data analysis

All raw data processing and measurements were performed using Fiji software, as described in Yoshida et al. (2022).

Moss size. The moss images were outlined automatically, and the area was measured using the Fiji software.

Tip growth rate. Time-lapse epifluorescent images of the protonemata were obtained every 10 min using a 10× lens. Kymographs were created along the axes of the growing caulonemal filaments, and the growth rate was obtained by measuring the slope of the kymographs.

Branch growth rate. Time-lapse images of protonemata with bulges were obtained every 10 min using a z-series taken every 5 μm for a range of 50 μm with a 60× lens. The branch length (between the tip and the basal cell wall) was measured at each time point.

Gametophore initial cell. Time-lapse images of gametophore initial cells were obtained every 6 min using a z-series taken every 2.5 μm for a range of

20 μm with a 60× lens, followed by the quantification of the morphological and temporal properties of the cells.

Image presentation. All images taken by fluorescent microscopy were shown in figures by maximum intensity projection.

Statistical analysis. Welch's two-tailed *t*-test was used when the samples to be compared comprised two groups. Tukey's multiple comparison test was used to analyze the datasets that included more than two groups. All statistical analyses were performed using R software. The data distribution was assumed to be normal, but this was not formally tested. The obtained *P*-values are denoted as follows: $^{*}P < 0.05$, $^{**}P < 0.01$, $^{***}P < 0.001$ and $^{****}P < 0.0001$. Unless otherwise stated, data from multiple experiments were combined because of insufficient sample numbers in a single experiment.

Supplementary Data

Supplementary data are available at *PCP* online.

Data Availability

The sequence data reported in this paper have been submitted to the DNA Data Bank of the Japan Sequence Read Archive under accession number PRJDB14224. The moss MO25A gene sequences used are available in Phytozome under the accession numbers Pp3c17_23520 (*PpMO25A1*) and Pp3c2_380 (*PpMO25A2*).

Funding

Japanese Society for the Promotion of Science (JSPS) KAKENHI (17H06471 to G.G. and Y.S. and 22H02644 and 22H04717 to G.G.); pre-doctoral fellowship of the JSPS to M.W.Y.; Open Access publication funded by KAKENHI grant number 22H04904.

Acknowledgements

The mutant line *08T6S44* was kindly provided by Dr. Yasuo Nagato (University of Tokyo). We are grateful to the members of the Laboratory of Plant Genetics at the National Institute of Genetics for their help with the cultivation of materials and Momoko Nishina, Maya Hakozaki, Chiemi Koketsu and Rie Inaba (Nagoya University) for their technical support.

Author Contributions

Projects were designed by K.N.T., M.W.Y., G.G. and Y.S.; material preparation, experiments and data analysis were performed by K.N.T., M.W.Y., T.T., S.S.-S., M.N.-T. and Y.S.; RNA-seq data were obtained by A.T.; Next Generation Sequencing (NGS) mapping was conducted by T.S.; the final data for publication were prepared by K.N.T. and M.W.Y. and the manuscript was written by K.N.T., M.W.Y., G.G. and Y.S. on behalf of all authors.

Disclosures

The authors have no conflicts of interest to declare.

References

Ashton, N.W. and Cove, D.J. (1977) The isolation and preliminary characterisation of auxotrophic and analogue resistant mutants of the moss, *Physcomitrella patens*. *Molec. Gen. Genet.* 154: 87–95.

Beutelmann, P. and Bauer, L. (1977) Purification and identification of a cytokinin from moss callus cells. *Planta* 133: 215–217.

Bidlingmaier, S., Weiss, E.L., Seidel, C., Drubin, D.G. and Snyder, M. (2001) The Cbk1p pathway is important for polarized cell growth and cell separation in *Saccharomyces cerevisiae*. *Mol. Cell Biol.* 21: 2449–2462.

Bizotto, F.M., Ceratti, R.S., Braz, A.S.K. and Masuda, H.P. (2018) Evolutionary history of Mo25 gene in plants, a component of RAM/MOR signaling network. *Mech. Dev.* 153: 64–73.

Bopp, M. (1963) Development of the protonema and bud formation in mosses. *Bot. J. Linn. Soc.* 58: 305–309.

Bridges, C.B. and Morgan, T.H. (1923) The Third-Chromosome Group of Mutant Characters of *Drosophila melanogaster*, Vol. 327. pp. 1–251. Carnegie Institution of Washington Publication, Washington, D.C.

Chien, S.-C., Brinkmann, E.-M., Teuliere, J. and Garriga, G. (2013) *Caenorhabditis elegans* PIG-1/MELK acts in a conserved PAR-4/LKB1 polarity pathway to promote asymmetric neuroblast divisions. *Genetics* 193: 897–909.

Collonnier, C., Epert, A., Mara, K., Maclot, F., Guyon-Debast, A., Charlot, F., et al. (2017) CRISPR-Cas9-mediated efficient directed mutagenesis and RAD 51-dependent and RAD 51-independent gene targeting in the moss *Physcomitrella patens*. *Plant Biotech. J.* 15: 122–131.

Cove, D.J. and Knight, C.D. (1993) The moss *Physcomitrella patens*, a model system with potential for the study of plant reproduction. *Plant Cell* 5: 1483–1488.

Davis, E.L., Rennie, P. and Steeves, T.A. (1979) Further analytical and experimental studies on the shoot apex of *Helianthus annuus*: variable activity in the central zone. *Can. J. Bot.* 57: 971–980.

de Jager, S.M., Maughan, S., Dewitte, W., Scofield, S. and Murray, J.A.H. (2005) The developmental context of cell-cycle control in plants. *Semin. Cell Dev. Biol.* 16: 385–396.

Dettmann, A., Illgen, J., März, S., Schürg, T., Fleissner, A. and Seiler, S. (2012) The NDR kinase scaffold HYM1/MO25 is essential for MAK2 map kinase signaling in *Neurospora crassa*. *PLoS Genet.* 8: e1002950.

Dobin, A., Davis, C.A., Schlesinger, F., Drenkow, J., Zaleski, C., Jha, S., et al. (2013) STAR: ultrafast universal RNA-Seq aligner. *Bioinformatics* 29: 15–21.

Filippi, B.M., de Los Heros, P., Mehellou, Y., Navratilova, I., Gourlay, R., Deak, M., et al. (2011) MO25 is a master regulator of SPAK/OSR1 and MST3/MST4/YSK1 protein kinases. *EMBO J.* 30: 1730–1741.

Goshima, T., Kume, K., Koyano, T., Ohya, Y., Toda, T. and Hirata, D. (2010) Fission yeast germinal center (GC) kinase Ppk11 interacts with Pmo25 and plays an auxiliary role in concert with the morphogenesis Orb6 network (MOR) in cell morphogenesis. *J. Biol. Chem.* 285: 35196–35205.

Hahn, H. and Bopp, M. (1968) A cytokinin test with high specificity. *Planta* 83: 115–118.

Hemerly, A.S., Ferreira, P.C., Van Montagu, M., Engler, G. and Inzé, D. (2000) Cell division events are essential for embryo patterning and morphogenesis: studies on dominant-negative cdc2aAt mutants of *Arabidopsis*. *Plant J.* 23: 123–130.

Hiei, Y., Ohta, S., Komari, T. and Kumashiro, T. (1994) Efficient transformation of rice (*Oryza sativa* L.) mediated by *Agrobacterium* and sequence analysis of the boundaries of the T-DNA. *Plant J.* 6: 271–282.

Hong, S.-K., Aoki, T., Kitano, H., Satoh, H. and Nagato, Y. (1995) Phenotypic diversity of 188 rice embryo mutants. *Dev. Genet.* 16: 298–310.

Horiguchi, G. and Tsukaya, H. (2011) Organ size regulation in plants: insights from compensation. *Front. Plant Sci.* 2: 24.

Inzé, D. and De Veylder, L. (2006) Cell cycle regulation in plant development. *Annu. Rev. Genet.* 40: 77–105.

Ishimoto, K., Sohonahra, S., Kishi-Kaboshi, M., Itoh, J.-I., Hibara, K.-I., Sato, Y., et al. (2019) Specification of basal region identity after asymmetric zygotic division requires mitogen-activated protein kinase 6 in rice. *Development* 146: dev176305.

Itoh, J.-I., Kitano, H., Matsuoka, M. and Nagato, Y. (2000) Shoot organization genes regulate shoot apical meristem organization and the pattern of leaf primordium initiation in rice. *Plant Cell* 12: 2161–2174.

Itoh, J.-I., Nonomura, K.-I., Ikeda, K., Yamaki, S., Inukai, Y., Yamagishi, H., et al. (2005) Rice plant development: from zygote to spikelet. *Plant Cell Physiol.* 46: 23–47.

Itoh, J.-I., Sato, Y., Sato, Y., Hibara, K.-Y., Shimizu-Sato, S., Kobayashi, H., et al. (2016) Genome-wide analysis of spatio-temporal gene expression patterns during early embryogenesis in rice. *Development* 143: 1217–1227.

Jakoby, M. and Schnittger, A. (2004) Cell cycle and differentiation. *Curr. Opin. Plant Biol.* 7: 661–669.

Jaspersen, S.L., Charles, J.F., Tinker-Kulberg, R.L. and Morgan, D.O. (1998) A late mitotic regulatory network controlling cyclin destruction in *Saccharomyces cerevisiae*. *Mol. Biol. Cell* 9: 2803–2817.

Jenik, P.D., Jurkuta, R.E.J. and Barton, M.K. (2005) Interactions between the cell cycle and embryonic patterning in *Arabidopsis* uncovered by a mutation in DNA polymerase ε. *Plant Cell* 17: 3362–3377.

Kanai, M.I., Okabe, M. and Hiromi, Y. (2005) seven-up Controls switching of transcription factors that specify temporal identities of *Drosophila* neuroblasts. *Dev. Cell* 8: 203–213.

Kofuji, R. and Hasebe, M. (2014) Eight types of stem cells in the life cycle of the moss *Physcomitrella patens*. *Curr. Opin. Plant Biol.* 17: 13–21.

Kouchi, H. and Hata, S. (1993) Isolation and characterization of novel nodulin cDNAs representing genes expressed at early stages of soybean nodule development. *Mol. Gen. Genet.* 238: 106–119.

Lopez-Obando, M., Hoffmann, B., Géry, C., Guyon-Debast, A., Téoulé, E., Rameau, C., et al. (2016) Simple and efficient targeting of multiple genes through CRISPR-Cas9 in *Physcomitrella patens*. *G3* 6: 3647–3653.

Maerz, S. and Seiler, S. (2010) Tales of RAM and MOR: NDR kinase signaling in fungal morphogenesis. *Curr. Opin. Microbiol.* 13: 663–671.

Marygold, S.J., Roote, J., Reuter, G., Lambertsson, A., Ashburner, M., Millburn, G.H., et al. (2007) The ribosomal protein genes and *Minute* loci of *Drosophila melanogaster*. *Genome Biol.* 8: R216.

Mehellou, Y., Alessi, D.R., Macartney, T.J., Szklarz, M., Knapp, S. and Elkins, J.M. (2013) Structural insights into the activation of MST3 by MO25. *Biochem. Biophys. Res. Comm.* 431: 604–609.

Meinke, D.W. (2020) Genome-wide identification of EMBRYO-DEFECTIVE (EMB) genes required for growth and development in *Arabidopsis*. *New Phytol.* 226: 306–325.

Mendoza, M., Redemann, S. and Brunner, D. (2005) The fission yeast MO25 protein functions in polar growth and cell separation. *Eur. J. Cell Biol.* 84: 915–926.

Mikami, M., Toki, S. and Endo, M. (2015) Comparison of CRISPR/Cas9 expression constructs for efficient targeted mutagenesis in rice. *Plant Mol. Biol.* 88: 561–572.

Miranda-Saavedra, D. and Barton, G.J. (2007) Classification and functional annotation of eukaryotic protein kinases. *Proteins* 68: 893–914.

Nakaoka, Y., Miki, T., Fujioka, R., Uehara, R., Tomioka, A., Obuse, C., et al. (2012) An inducible RNA interference system in *Physcomitrella patens* reveals a dominant role of augmin in phragmoplast microtubule generation. *Plant Cell* 24: 1478–1493.

Nelson, B., Kurischko, C., Horecka, J., Mody, M., Nair, P., Pratt, L., et al. (2003) RAM: a conserved signaling network that regulates Ace2p transcriptional activity and polarized morphogenesis. *Mol. Biol. Cell* 14: 3782–3803.

Neto-Silva, R.M., de Beco, S. and Johnston, L.A. (2010) Evidence for a growth-stabilizing regulatory feedback mechanism between Myc and Yorkie, the *Drosophila* homolog of Yap. *Dev. Cell* 19: 507–520.

Nosaka-Takahashi, M., Kato, M., Kumamaru, T. and Sato, Y. (2022) Measurements of the number of specified and unspecified cells in the shoot apical meristem during a plastochron in rice (*Oryza sativa*) reveal the robustness of cellular specification process in plant development. *PLoS One* 17: e0269374.

Ohnishi, T., Yoshino, M., Yamakawa, H. and Kinoshita, T. (2011) The biotron breeding system: a rapid and reliable procedure for genetic studies and breeding in rice. *Plant Cell Physiol.* 52: 1249–1257.

Oud, B., Guadalupe-Medina, V., Nijkamp, J.F., de Ridder, D., Pronk, J.T., van Maris, A.J.A., et al. (2013) Genome duplication and mutations in ACE2 cause multicellular, fast-sedimenting phenotypes in evolved *Saccharomyces cerevisiae*. *Proc. Natl. Acad. Sci. USA* 110: E4223–31.

Pan, D. (2010) The hippo signaling pathway in development and cancer. *Dev. Cell* 19: 491–505.

Pringle, J.R. and Hartwell, L.H. (1981) The *Saccharomyces cerevisiae* cell cycle. *In* The Molecular Biology of the Yeast Saccharomyces: Life Cycle and Inheritance. Edited by Strathern, J.N., Jones, E.W. and Broach, J.R. pp. 97–142. Cold Spring Harbour Laboratory, Cold Spring Harbour, NY.

Rademacher, E.H. and Offringa, R. (2012) Evolutionary adaptations of plant AGC kinases: from light signaling to cell polarity regulation. *Front. Plant Sci.* 3: 250.

Rahman, M.H., Toda, E., Kobayashi, M., Kudo, T., Koshimizu, S., Takahara, M., et al. (2019) Expression of genes from paternal alleles in rice zygotes and involvement of OsASGR-BBML1 in initiation of zygotic development. *Plant Cell Physiol.* 60: 725–735.

Reddy, G.V., Heisler, M.G., Ehrhardt, D.W. and Meyerowitz, E.M. (2004) Real-time lineage analysis reveals oriented cell divisions associated with morphogenesis at the shoot apex of *Arabidopsis thaliana*. *Development* 131: 4225–4237.

Reski, R. and Abel, W.O. (1985) Induction of budding on chloronemata and caulonemata of the moss, *Physcomitrella patens*, using isopentenyladenine. *Planta* 165: 354–358.

Robinson, M.D., McCarthy, D.J. and Smyth, G.K. (2010) EdgeR: a bioconductor package for differential expression analysis of digital gene expression data. *Bioinformatics* 26: 139–140.

Ronceret, A., Guilleminot, J., Lincker, F., Gadea-Vacas, J., Delorme, V., Bechtold, N., et al. (2005) Genetic analysis of two *Arabidopsis* DNA polymerase epsilon subunits during early embryogenesis. *Plant J.* 44: 223–236.

Sakamoto, Y., Ishimoto, A., Sakai, Y., Sato, M., Nishihama, R., Abe, K., et al. (2022) *Commun. Biol.* 5: 12.

Saputo, S., Chabrier-Rosello, Y., Luca, F.C., Kumar, A. and Krysan, D.J. (2012) The RAM network in pathogenic fungi. *Eukaryot. Cell* 11: 708–717.

Surana, U., Amon, A., Dowzer, C., McGrew, J., Byers, B. and Nasmyth, K. (1993) Destruction of the CDC28/CLB mitotic kinase is not required for the metaphase to anaphase transition in budding yeast. *EMBO J.* 12: 1969–1978.

Suzuki, T., Kawai, T., Takemura, S., Nishiwaki, M., Suzuki, T., Nakamura, K., et al. (2018) Development of the Mitsucal computer system to identify causal mutation with a high-throughput sequencer. *Plant Reprod.* 31: 117–128.

Takahashi, H., Kamakura, H., Sato, Y., Shiono, K., Abiko, T., Tsutsumi, N., et al. (2010) A method for obtaining high quality RNA from paraffin sections of plant tissues by laser microdissection. *J. Plant Res.* 123: 807–813.

Tang, H., Duijts, K., Bezanilla, M., Scheres, B., Vermeer, J.E.M. and Willemsen, V. (2020) Geometric cues forecast the switch from two- to three-dimensional growth in *Physcomitrella patens*. *New Phytol.* 225: 1945–1955.

ten Hove, C.A., Lu, K.-J. and Weijers, D. (2015) Building a plant: cell fate specification in the early *Arabidopsis* embryo. *Development* 142: 420–430.

ten Klooster, J.P., Jansen, M., Yuan, J., Oorschot, V., Begthel, H., Giacomo, V.D., et al. (2009) Mst4 and Ezrin induce brush borders downstream of the Lkb1/Strad/Mo25 polarization complex. *Dev. Cell* 16: 551–562.

Thompson, B.J. and Sahai, E. (2015) MST kinases in development and disease. *J. Cell Biol.* 210: 871–882.

Vidali, L., Augustine, R.C., Kleinman, K.P. and Bezanilla, M. (2007) Profilin is essential for tip growth in the moss *Physcomitrella patens*. *Plant Cell* 19: 3705–3722.

Weiss, E.L. (2012) Mitotic exit and separation of mother and daughter cells. *Genetics* 192: 1165–1202.

Weiss, E.L., Kurischko, C., Zhang, C., Shokat, K., Drubin, D.G. and Luca, F.C. (2002) The *Saccharomyces cerevisiae* Mob2p-Cbk1p kinase complex promotes polarized growth and acts with the mitotic exit network to facilitate daughter cell-specific localization of Ace2p transcription factor. *J. Cell Biol.* 158: 885–900.

Yamada, M., Miki, T. and Goshima, G. (2016) *Imaging Mitosis in the Moss Physcomitrella patens*. *In* The Mitotic Spindle: Methods and Protocols. Edited by Chang, P. and Ohi, R. pp. 263–282. Springer, New York, NY.

Yi, P. and Goshima, G. (2020) Rho of plants GTPases and cytoskeletal elements control nuclear positioning and asymmetric cell division during *Physcomitrella patens* branching. *Curr. Biol.* 30: 2860–2868.e3.

Yoshida, M.W., Hakozaki, M. and Goshima, G. (2022) Armadillorepeat-containing kinesin represents the versatile plus-end-directedtransporter in plants. bioRxiv 499244.

Zermiani, M., Begheldo, M., Nonis, A., Palme, K., Mizzi, L., Morandini, P., et al. (2015) Identification of the Arabidopsis RAM/MOR signalling network: adding new regulatory players in plant stem cell maintenance and cell polarization. *Ann. Bot.* 116: 69–89.

Zhao, B., Tumaneng, K. and Guan, K.L. (2011) The Hippo pathway in organ size control, tissue regeneration and stem cell self-renewal. *Nat. Cell Biol.* 13: 877–883.

Ziosi, M., Baena-López, L.A., Grifoni, D., Froldi, F., Pession, A., Garoia, F., et al. (2010) dMyc functions downstream of Yorkie to promote the supercompetitive behavior of hippo pathway mutant cells. *PLoS Genet.* 6: e1001140.